XAFS Investigation of Pu(IV) Hydrolysis Products

M.A. Denecke, V. Neck, J. Rothe
Institut für Nukleare Entsorgung, Forschungszentrum Karlsruhe, Karlsruhe, Germany

Introduction

A knowledge of actinide solubility in aqueous media is indispensable for predictive modeling of actinide migration in the environment. Because of the strong tendency of tetravalent actinides toward hydrolysis and polynucleation, the presence of colloids has led to contradictory solubility data reported for actinide oxo/hydroxide [$An(IV)O_n(OH)_{4-2n}\cdot xH_2O$] phases. The goal of the present study is to follow changes in Pu(IV) coordination by Pu L3 x-ray absorption fine structure (XAFS) of samples similar to those used for Pu(IV) solubility measurements with combined laser-induced breakdown detection (LIBD)/coulometric pH titration.

Methods and Materials

A Pu(IV) stock solution was prepared from a Pu(VI) stock solution by bubbling NO through it. The concentration of the Pu(VI) solution was determined from its uv/visible absorption spectrum to be 16.1 mM Pu(VI) in 1 M HCl. Utmost care was taken to avoid oxygen in the samples. All of the aqueous reagents were prepared from oxygen-free water. The Pu(IV) solution samples were prepared in a N_2-purged glove bag. Following the experiments, a control uv/visible is measurement of the pH 1.3 sample (Sample A, see Table 1) was performed. No evidence of oxidation was observed. Solid, freshly precipitated $Pu(OH)_4$ was separated from the aqueous solution by ultrafiltration and collected on a cellulose triacetate membrane microfilter. The filter with the wet solid was encased inside a thin latex bag. The stock solution, the samples with 10 times more dilute Pu(IV) solution, and the precipitate (Table 1) were investigated with XAFS. Measurements of their Pu L3 XAFS spectra were performed at the BESSRC beamline 12-BM by using a Si<111> double-crystal monochromator and a beam spot of 0.5 mm^2. The incident beam was free of higher harmonic reflections, as shown by the absence of the corresponding inelastic scattering peaks recorded with an energy-dispersive detector. The spectra were calibrated against the first-derivative x-ray absorption near-edge structure (XANES) spectrum of a Zr foil, defined as 17.998 keV. Spectra were recorded in both transmission and fluorescence mode. Argon-filled ionization chambers were used for transmission spectra detection, and a 13-element energy-dispersive solid-state Ge detector was used for fluorescence spectra. All solution samples were contained in capped polyethylene vials (4-mm inner diameter), with the caps taped with a thick layer of parafilm to prevent oxygen intrusion. All samples were mounted in the Actinide Facility's sample changer for transport and measurement. Three to seven scans were collected and averaged for each sample.

TABLE 1. Summary of samples.

ID	Sample Description
A	16.1 mM Pu(IV) in 0.4 M HCl
B	1 mM Pu(IV) in 1M $HClO_4$, $-\log[H^+] = 0$
C	1 mM Pu(IV) in 0.5 M NaCl, $-\log[H^+] = 0.56$
D	1 mM Pu(IV) in 0.5 M NaCl, $-\log[H^+] = 0.93$
E	1 mM Pu(IV) in 0.5 M NaCl, $-\log[H^+] = 1.27$
F	1 mM Pu(IV) in 0.5 M NaCl, $-\log[H^+] = 1.38$
G	1.75 mM Pu(IV) in 0.5 M NaCl, $-\log[H^+] = 1.75$
H	Precipitated $Pu(OH)_4$ (am)

XAFS data analysis was based on standard least squares fitting techniques by using the WinXAS [1] and UWXAFS [2] program packages. The region up to about 700 eV above the Pu L3 edge (k of ~13 Å-1) of the spectra taken in fluorescence mode was investigated. The k^2-weighted data were fit with cubic spline functions to obtain the atomic background function $\mu_0(E)$ for the subsequent extraction of $\chi(k)$. The ionization energy E_0 was fixed at the maximum of the white line (WL) in the individual spectra at ~18,068 eV. Metric parameters (neighboring atomic distances R_i, mean square radial displacements or EXAFS Debye-Waller factors σ^2_i, and coordination numbers N_i for the different coordination shells) were determined by using the FEFFIT code. Backscattering amplitude and phase shift functions for single scattering paths in a three-shell PuO_2 cluster (fluorite structure) were obtained from FEFF8.2 [3] calculations. All fitting operations were performed in R-space. The amplitude reduction factor S_0^2 was fixed at 1. XANES spectra for samples A-H were isolated from XAFS scans following subtraction of the pre-edge background absorption, approximated as a linear function, and normalized. In order to quantify the WL intensity in these spectra, curve-fitting was accomplished by modeling the experimental data by using pseudo-Voigt (WL), Gaussian (first EXAFS feature around 18,105 eV), and arctan (edge-step) functions.

Results

The k^2-weighted EXAFS-functions $\chi(k)$ are shown in Fig. 1 at the left, and the corresponding Fourier transform (FT) magnitudes are shown at the right. All spectra exhibit an intense, more or less asymmetric FT peak at ~1.9 Å, corresponding to a phase-corrected distance value of about 2.4 Å. This peak represents oxygen atoms that make up the first coordination sphere of the central absorbing Pu(IV) in all samples. The EXAFS metrical parameters obtained from fits of experimental data to the EXAFS equation are summarized in Table 2. Sample A is the stock solution, and samples B and H are the Pu^{4+}aquo ion and solid $Pu(OH)_4$ precipitate as reference compounds. Spectra of samples C-G monitor eigencolloid formation and changes in the colloidal suspensions after the solubility threshold has been crossed when -log[H^+] is successively increased. Only sample B (1 mM Pu(IV) in 1M $HClO_4$, -log[H^+] = 0) exhibits a spectrum dominated by a single, dampened sinusoidal contribution, originating from backscattering on a single shell of oxygen atoms. All other spectra exhibit a more complex absorption fine structure. This includes

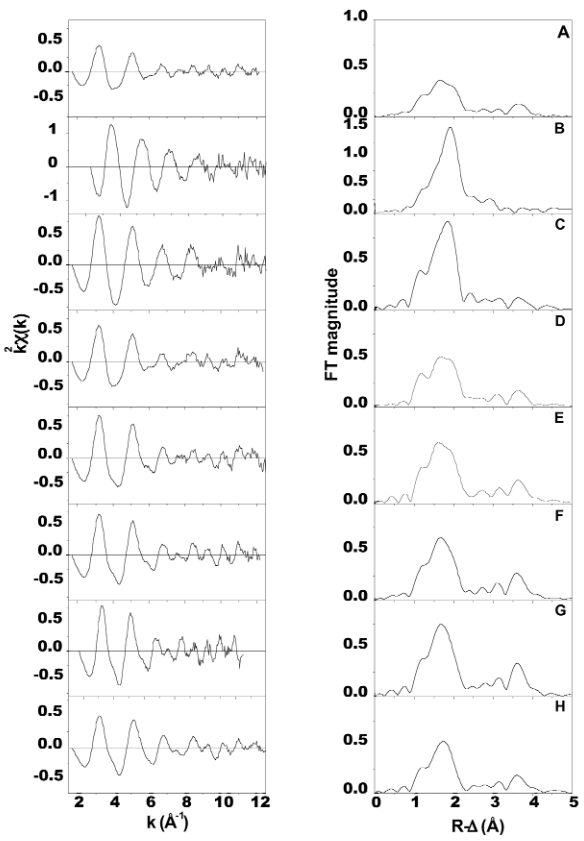

FIG. 1. k^2-weighted $\chi(k)$-functions of the samples listed in Table 1 (left panel), and corresponding Fourier transform magnitudes (right panel). Note the different ordinate scale for sample B

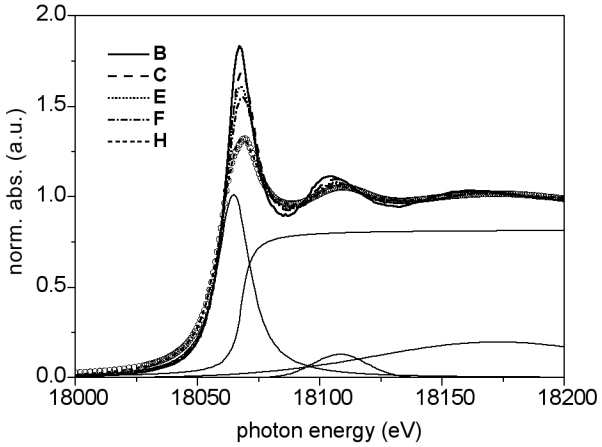

FIG. 2. Pu L3 edge XANES spectra for Pu^{4+}aquo ion (B), Pu(IV) hydroxide colloids (C, E, F), and precipitated $Pu(OH)_4$(am) (H), including least-squares fit (open circles) and fit components for sample H.

the appearance of a high-frequency EXAFS contribution, which is found in the fit procedure to be associated with a Pu-Pu interaction. The normalized XANES spectra for samples B, C, E, F, and H are depicted in Fig. 2. A significant change in the intensity and width of the WL feature is observed. The intensity decreases going from the Pu^{4+}aquo ion (B) to the amorphous $Pu(OH)_4$ precipitate (H). There is an almost linear correlation between the drop of WL intensity (determined as the pseudo-Voigt profile height) and -log[H^+]. The pseudo-Voigt profile area, reflecting the integral $2p_{3/2} \rightarrow 6d$ transition probability, remains constant for all samples. The stock solution (A) and the solid $Pu(OH)_4$ (amorphous) (H) exhibit the lowest WL intensities.

Discussion

The metric parameters obtained for 1 mM Pu(IV) at -log[H^+] = 0 (B) are those of the Pu^{4+}aquo ion: 8-9 water molecules (depending on the uncertainty in the S_0^2 value) coordinated to Pu(IV) at a Pu-O bond distance of 2.38 ± 0.02 Å. The highly asymmetric oxygen coordination in the colloid samples A and C-G and the amorphous precipitate H indicates the presence of different Pu-O bond lengths from different coordinating oxygen atoms ($-O^-$, -OH, OH_2). Samples D-G exhibit splitting of the Pu-O shell into a dominant oxygen contribution at distances slightly longer than that expected for PuO_2 (crystalline) [4] and a smaller contribution at a significantly shorter distance (around 2.22 Å). Only for sample A (the colloids formed in the concentrated stock solution) does the short distance contribution seem to be dominant. We assign this shorter Pu-O distance to hydroxyl groups, whereas the

Table 2. Data range and metric parameters from least-squares fitting analysis of EXAFS spectra

ID	Fit Range R-Δ (Å)	Shell	R (Å)	N	σ^2 (Å2)	ΔE (eV)	*R*-Factor
A	1.34-4.02	O1	2.24	3.3	0.0031	3.07	0.005
		O2	2.42	0.8	0.0099	3.07	
		Pu	3.86	2.1	0.0076	3.19	
B	1.32-2.67	O	2.38	8.4	0.0077	8.3	0.004
C	1.32-4.08	O	2.35	7.2	0.0094	1.06	0.007
		Pu	3.90	1.9	0.0067	4.64	
D	1.35-4.0	O1	2.20[a]	1.1	0.0004	3.10	0.007
		O2	2.42	4.4	0.0068	3.10	
		Pu	3.90	3.0	0.0085	4.52	
E	1.32-3.96	O1	2.22	0.7	0.0012	2.77	0.013
		O2	2.38	5.6	0.0122	2.77	
		Pu	3.85	4.3	0.0090	2.08	
F	1.35-3.99	O1	2.22	1.5	0.0017	2.51	0.008
		O2	2.39	4.0	0.0059	2.51	
		Pu	3.87	4.2	0.0075	1.71	
G	1.32-3.96	O1	2.29	1.4	0.0080	3.08	0.008
		O2	2.37	5.0	0.0136	3.08	
		Pu	3.87	4.9	0.0075	1.74	
H	1.35-3.99	O	2.32	4.0	0.0104	2.38	0.016
		Pu	3.87	2.4	0.0066	1.84	

[a] Fixed value.

elongated Pu-O distance is assigned to the Pu-O-Pu "backbone" in the nanoparticle lattice. The apparent disorder in the Pu-O shell varies with -log[H^+], probably because of the varying surface-to-bulk ratio and, hence, surface tension and structural strain. In contrast, the Pu-Pu distances are hardly influenced by these fluctuations. This supports the hypothesis of a rather rigid lattice, with its -Pu-O-Pu- backbone forming the basis of the polynuclear and colloidal Pu(IV) hydrolysis species.

The WL intensity variation results from a distinct particle size effect [5]). Of all the Pu(IV) samples investigated here, the Pu^{4+}aquo ion can be assumed to have the most molecular orbital (MO)-like 6*d* final state. Because the $2p_{3/2} \rightarrow 6d$ dipole-allowed transition probability is proportional to the energy-dependent density of the 6*d* final states, the MO-like more-localized final state has the greatest transition probability of these samples and, hence, the largest WL. The 6*d* state of the condensed amorphous $Pu(OH)_4$(am) precipitate is better described as a band. The density of the 6*d*-like final state is spread over a larger energy interval. The WL height is observed to be lowest for this sample as a result of the spread of 6*d*-like final state energies (i.e., a band). For the same reason, the width of the WL feature increases significantly with decreasing height (Fig. 2). The colloid samples C-G represent an intermediate situation. These samples exhibit decreasing WL heights and increasing peak widths, which reflect an increase in particle size with increasing extent of hydrolysis (increasing -log[H^+]).

Acknowledgments

Use of the APS was supported by the U.S. Department of Energy, Office of Science, Office of Basic Energy Sciences, under Contract No. W-31-109-ENG-38. We are grateful for beam time allotment and experimental assistance from the BESSRC beamline staff. Use of the infrastructures of the Actinide Facility in the Chemistry Division of Argonne National Laboratory for synchrotron research and support from the Chemistry Division staff are also acknowledged with gratitude.

References

[1] T. Ressler, J. Physique IV **7-C2**, 269 (1997).
[2] E.A. Stern, M. Newville, B. Ravel, Y. Yacoby, D. Haskel, Physica B **208** and **209**, 117-120 (1995).
[3] A.L. Ankudinov, B. Ravel, J.J. Rehr, and S.D. Conradson, Phys. Rev. B **58**, 7565-7576 (1998).
[4] J. Rothe, M.A. Denecke, V. Neck, R. Müller, and J.I. Kim, Inorg. Chem. **41**, 249-258 (2002).
[5] L. Koch, "Plutonium and plutonium compounds," in Ullmann's Encyclopedia of Industrial Chemistry (Wiley-VCH, 2000).